THE JOURNAL OF PHYSICAL CHEMISTRY C

Article

Cite This: J. Phys. Chem. C 2019, 123, 9001−9012

pubs.acs.org/JPCC

Effect of Structural Evolution of Gold Species Supported on Ceria in Catalyzing CO Oxidation

Xiu-Ling Wang,[†] Xin-Pu Fu,[†] Wei-Wei Wang,[†] Chao Ma,[*,§] Rui Si,[*,‡] and Chun-Jiang Jia[*,†]

[†]Key Laboratory for Colloid and Interface Chemistry, Key Laboratory of Special Aggregated Materials, School of Chemistry and Chemical Engineering, Shandong University, Jinan 250100, People's Republic of China

[‡]Shanghai Synchrotron Radiation Facility, Shanghai Institute of Applied Physics, Chinese Academy of Sciences, Shanghai 201204, People's Republic of China

[§]College of Materials Science and Engineering, Hunan University, Changsha 410082, People's Republic of China

Supporting Information

ABSTRACT: The intrinsic reactivity of atomically dispersed gold catalysts for low-temperature (L-T) CO oxidation remains an elusive issue. Here, two kinds of atomically dispersed gold with different loadings supported on nanoceria prepared via a deposition precipitation method were evaluated as catalysts for L-T CO oxidation. Much distinct differences in catalyzing CO oxidation behaviors were exhibited on the two kinds of gold catalysts. These weakly anchored gold species in the 1% Au/CeO_2 (1 wt % gold loading) catalyst revealed increasing reactivity under the reaction condition, while these strongly anchored ones in the 0.5% Au/CeO_2 (0.5 wt % gold loading) catalyst were inactive. For the 1% Au/CeO_2 catalyst, in situ diffuse reflectance infrared spectroscopy (DRIFTS) proved gold species transformation from Au^{n+} ($1 \le n < 3$) to $Au^{\delta+}$ ($0 < \delta < 1$), and simultaneously, aberration-corrected scanning transmission electron microscope measurements confirmed that partial atomically dispersed gold species transformed into gold clusters. While for 0.5% Au/CeO_2, atomically dispersed Au^{n+} ($1 \le n < 3$) hardly varied in catalyzing CO oxidation at room temperature (RT). CO adsorption tests by in situ DRIFTS combining with the kinetics measurements demonstrated that these formed $Au^{\delta+}$ sites were much superior in adsorbing CO molecules than monodispersed Au^{n+} atoms at RT. Therefore, the gap in capturing CO molecules intrinsically resulted in the distinct catalytic performance for clustered $Au^{\delta+}$ ($0 < \delta < 1$) and atomically dispersed Au^{n+} ($1 \le n < 3$).

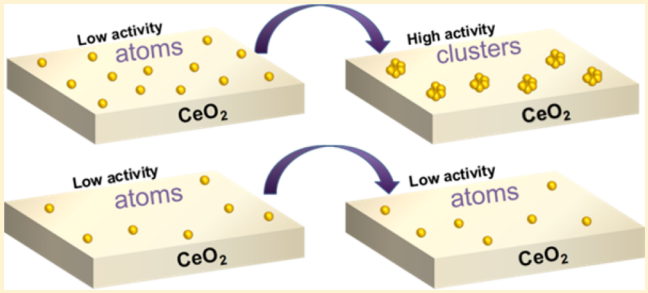

1. INTRODUCTION

Because the pioneering research on small-size Au species, ultra-active for CO oxidation, was discovered by Haruta in 1987,[1] more and more scientists have been attracted to reveal the structural−function relation of supported gold catalysts.[2−5] Thus far, people have indicated that the states of gold species,[6,7] the redox properties of the support,[8,9] and the interactions between gold species and matrix materials,[10] strongly influenced catalytic performance. Among them, the authentic contributions of gold in various states that include nanoparticles (NPs), clusters, and single atoms (SAs) to the catalytic activity were under debate.[11,12] For the gold particles and gold clusters, which are mainly rich in metallic surface sites, the high-active nature of them in catalyzing CO oxidation has been revealed.[13−16] Besides gold particles and clusters, gold single atoms have also attracted great interest.[17−21] SAs catalysts (SACs) can achieve the ultimate goal of fine dispersion[18−20] and maximize the utilization of metal atoms, which is especially important for supported noble metal catalysts.[21] However, single atoms stayed at a low-coordination environment including many unsaturated coordination sites, so the surface free energy of metal atoms is considerably high, leading to the formation of small clusters.[21,22] Therefore, limited by their instability and complexity under the reaction condition, the activity contributions of gold single atoms still remain intensely controversial.[23−25]

Zhang et al. reported that supported Au single atoms exhibited high activity and excellent stability for CO oxidation in the Au/FeO_x system.[26] They have reported that singly dispersed Au showed higher selectivity to CO oxidation and very low selectivity to H_2 oxidation at 80 °C, compared with corresponding Au clusters and NPs for CO-PROX reaction.[27] However, very little information concerning how CO and O_2 reacted on supported gold single atoms was mentioned. Li et al. proposed dynamic single atom catalysis based on theoretical simulations.[28,29] They thought gold atoms with the cationic state could break away from the gold NPs to catalyze the reaction and then reintegrated back to Au NPs after the CO oxidation reaction. Therefore, the dynamic Au single atoms served as the active sites in the catalytic process. However,

Received: January 4, 2019
Revised: February 24, 2019
Published: March 13, 2019

DOI: 10.1021/acs.jpcc.9b00096
J. Phys. Chem. C 2019, 123, 9001−9012

some reports also demonstrated that mononuclear cationic Au species were much less active for CO oxidation, compared with the small gold clusters and NPs.[30,31] As probed by operando diffuse reflectance infrared spectroscopy (DRIFTS) combined with quadruple mass spectrometry, Wu et al. found isolated Au atoms were inactive, while metallic Au species were extremely active for CO oxidation at room temperature (RT) in the Au/SiO_2 system.[32] Corma et al. compared reactivity from the perspective of activated oxygen.[33] Characterization of the spent sample indicated that the active species were not the isolated gold atoms presented in the as-prepared catalyst but were other metal species formed during the reaction. They thought isolated gold atoms cannot activate O_2, but small gold clusters are excellent catalysts for O_2 activation, according to the theoretical study of the reaction mechanism. Gates and Aguilar-Guerrero thought formation of clusters is beneficial for enhancement of activity.[30] Kinetics result was described quantitatively with apparent activation energy of the cluster only about one-third of the value of mononuclear gold complexes. Meanwhile, they believed that the real active site is gold clusters and the catalytic behavior observed with the sample incorporating the mononuclear gold complexes should be attributed to undetected gold clusters. Studies on model catalysts also suggested that Au single atoms were much inferior compared with the subnanometer-sized clusters in catalyzing CO oxidation.[34] Therefore, so far, the intrinsic activity of Au single atoms is still elusive.

There are two main challenges in authenticating the contribution of gold single atoms in catalyzing CO oxidation. One is the unstable nature of SA species, especially under a reductive reaction condition, which impeded a direct investigation of its intrinsic activity.[35,36] The other is difficult to fabricate comparable systems and effectively monitor their real structural information. In this work, atomically dispersed gold supported on the nanopolyhedron ceria was facilely fabricated via a deposition precipitation (DP) method with differing gold loadings (1% vs 0.5% in weight, named as 1% Au/CeO_2 and 0.5% Au/CeO_2, respectively). Tremendous distinction in catalyzing ambient CO oxidation revealed intrinsic difference of active sites. The catalytic reactivity of the 1% Au/CeO_2 catalyst was 4 times higher than that of 0.5% Au/CeO_2 (2000 vs 540 $mmol_{CO}\cdot g_{Au}^{-1}\cdot h^{-1}$) under the premise that CO conversion was controlled up to 12% at 40 °C by adjusting space velocity (SV). The in situ DRIFTS results showed that the clustered $Au^{\delta+}$ ($0 < \delta < 1$) species transformed from single Au atoms (1% Au/CeO_2) played a major role in catalyzing the reaction; while isolated Au^{n+} ($1 \leq n < 3$) species (0.5% Au/CeO_2) were spectators in the CO oxidation reaction at RT.

2. EXPERIMENTAL SECTION

2.1. Preparation of Ceria Support. The CeO_2 NP was prepared by using a surfactant-assisted coprecipitation method reported previously with minor alterations.[37] Typically, 6 mmol of the surfactant using cetyltrimethyl ammonium bromide was dispersed in ultrapure water (200 mL, resistance = 18.25 MΩ). Subsequently, 10 mmol of $Ce(NO_3)_3\cdot 6H_2O$ was added into the above slurry with gradual stirring. Then, the pH of the final solution around 9 was ensured by adjusting with NaOH (0.5 M) aqueous solution, and aged at 90 °C in the oil bath. The resultant precipitates were centrifuged and washed to remove the impurity ion and dried at 110 °C for 12 h. The obtained product was calcined in a muffle furnace at 400 °C for 4 h to get pale yellow CeO_2 powder.

2.2. Preparation of Gold−Ceria Catalysts. Au/CeO_2 catalysts with different weight percentages of Au were synthesized using a deposition−precipitation (DP) method by applying $HAuCl_4$ as the Au precursor.[38] In the typical experiment, 1.0 g of the CeO_2 support was dissolved in ultrapure water (50 mL, resistance = 18.25 MΩ) and stirred. Ammonium carbonate (2.4 g) was added. Then, the $HAuCl_4$ solution (0.0125 M) was added drop by drop under constant stirring. Stirring was performed for 20 min at RT to adequately mix and then aged for 1 h. The slurry was filtered and washed, followed by drying at 70 °C for 3 h. The as-prepared samples are denoted as 0.5% Au/CeO_2 and 1% Au/CeO_2.

2.3. Characterization Methods. Inductively coupled plasma (ICP) atom emission spectroscopy which was performed on an IRIS Intrepid II XSP instrument (Thermo Electron Corp.) was used to detect gold concentration.

The X-ray powder diffraction (XRD) test was analyzed on the PANalytical X'Pert3 type X-ray powder diffractometer (40 mA, 40 kV), with Cu Kα (λ = 1.5418 Å) as the radiation source. The scanning range of 2θ is from 10° to 90°, and the duration is 8 min.

The N_2 adsorption−desorption characterizations were investigated on a Builder SSA-4200 physical adsorption instrument at −196 °C. The sample was pretreated with vacuum degassing at 200 °C for 7 h before the test. The specific surface area was counted according to the Brunauer−Emmett−Teller (BET) equation.

High-resolution transmission electron microscopy images and elemental mapping were taken by using a FEI Tecnai F20 microscope operating at 200 kV. The atomic-resolution high-angle annular dark-field scanning transmission electron microscopy (HAADF−STEM) images were recorded on a JEOL ARM200F field-emission transmission electron microscope, which is equipped with a probe-forming aberration corrector and operated at 200 kV.

The valence of the element was analyzed by X-ray photoelectron spectroscopy (XPS) performed on ESCALAB 250Xi. The X-ray sources used in XPS experiments are XR6 (XR6 can continuously adjust the beam spot from 20 to 900 μm) and the beam spot is 500 μm. The power and spot selection are typical settings used by ESCALAB 250Xi. The binding energy scales were corrected by setting the C 1s transition at 284.5 eV.

Temperature-programmed reduction by hydrogen (H_2-TPR) was operated on a Builder PCSA-1000 instrument equipped with a thermal conductivity detector. The samples were heated from RT to 400 °C with a ramping rate of 10 °C·min^{-1} under 5% H_2/Ar mixed gas flow. Prior to experiments, the sieved sample (20−40 mesh, 30 mg) loaded in the U-type quartz tube reactor was activated at 300 °C for 30 min in a pure O_2 atmosphere.

The temperature-programmed reduction employing CO (CO-TPR) tests were monitored by online LC-D200M, TILON mass spectrometry (MS). The sample (100 mg) (20−40 mesh) was loaded into a quartz tube and activated at 300 °C for 30 min with a ramping rate of 10 °C·min^{-1} under an oxygen atmosphere. It was then cooled down to RT in He flow, it switched into 2% CO/He, and stabilization was maintained. After that, the catalyst was heated from RT to 800 °C. The temperature-programmed desorption by CO or CO_2 (CO-TPD/CO_2-TPD) tests was activated as described above.

DOI: 10.1021/acs.jpcc.9b00096
J. Phys. Chem. C 2019, 123, 9001−9012

Subsequently, desorbing adsorbed CO or CO_2 with ramping the temperature in He flow. CO (m/z = 28) and CO_2 (m/z = 44) signals in the outlet gas were analyzed by the MS detector.

The ex situ Raman spectrum was acquired on a LabRAM HR800 spectrometer (HORLBA JY) by activating Ar^+ laser (λ = 632 nm) at RT. The test region was set from 200 to 1000 cm^{-1} with 2 cm^{-1} for spectral resolution.

In situ diffuse reflectance infrared Fourier transform spectroscopy (DRIFTS) was conducted on a Bruker Vertex 70 FTIR spectrometer equipped with a mercury−cadmium−telluride detector cooled with liquid nitrogen. Prior to measurement, the fresh samples with 30 mg were activated in the same manner as the catalytic test and then cooled down to RT in N_2 flow; meanwhile, background spectra were collected at 4 cm^{-1} resolution. In the following CO adsorption measures, a "CO−N_2−CO−O_2" mode was carried out by DRIFTS. 2% CO was introduced for 30 min and then purged with N_2 or O_2; the real-time spectra were collected all the time. In typical CO oxidation experiments, the samples came into contact with the reaction gas (1% CO/20% O_2/N_2, flow rate: 30 mL·min^{-1}) at RT for 1 h and then was heated in the gradient way (25 °C/1 h) and maintained at target temperature. DRIFTS were collected by subtracting the background from raw data. Analysis of the spectra was operated by using OPUS software.

2.4. Activity Measurements. CO oxidation activity of the catalysts was investigated in a plug flow reactor weighing 50 mg of sieved samples (20−40 mesh) in a reaction mixture gas of 1% CO/20% O_2/N_2 (67 mL·min^{-1}, 99.997% purity), matched with a SV of 80 000 mL·g_{cat}^{-1}·h^{-1}. Prior to the reaction, the catalyst was activated in a fixed-bed reactor at 300 °C for 2 h, then cooled down to RT in pure N_2. The light-off catalytic activity test was heated up to 300 °C with a ramping rate of 2 °C·min^{-1} under the reaction condition. At the same time, to explore the stability of the catalysts, the samples were continuously tested for more than 10 h under the same catalytic atmosphere at 25 °C. The concentrations of CO and CO_2 in the output gas were detected online by nondispersive IR spectroscopy with Gasboard-3500, Wuhan Sifang Company of China.

2.5. Kinetics Tests. The kinetics measures were conducted in the same fixed-bed reactor as described above. The CO conversion was less than 15% in order to exclude the internal and external diffusion limitations (typically 2−5 mg of catalyst powder was diluted with quartz sand). Partial pressure of CO and O_2 was measured by adjusting the corresponding gas proportions, while keeping the total flow rate unchanging.

3. RESULTS

3.1. Morphology Information of Gold−Ceria Catalysts. Two kinds of gold−ceria catalysts with different gold loadings were prepared by the DP method. The concentrations of Au in both Au/CeO_2 catalysts measured by ICP-AES were 0.26 and 0.84 wt %, respectively (Table S1). The specific surface areas determined by the N_2 adsorption and BET analysis were 114.9, 105.8, and 93.1 m^2/g for the CeO_2 support, 0.5, and 1% Au/CeO_2, respectively (Figure S1). The polyhedron-like shape of the nanoceria matrix with a diameter of ∼9 nm was observed by HRTEM. No detectable Au particles or clusters were revealed on the surface of ceria nanopolyhedron (NP) for both catalysts (Figure S2). Atomic-resolution HAADF−STEM images were taken to reveal the detailed morphology of gold species. As shown in Figure 1, a few bright dots of atoms were exhibited for both as-prepared gold−ceria catalysts, indicating the monodispersed nature of Au species. Their XRD patterns showed the presence of the pure cubic fluorite CeO_2 phase (no. 34-0394), without any detectable diffraction peaks of crystalized Au species (Figure 2a) because of ultrafine Au particles or low Au loadings.[39,40] The elemental mapping results also confirmed that Au species homogeneously dispersed on the surface of CeO_2 NP, implying the ultrasmall size of gold species.

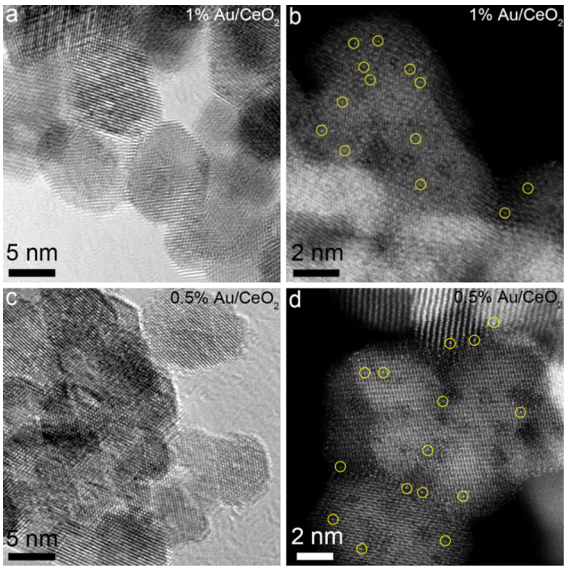

Figure 1. High-resolution TEM images and aberration-corrected HAADF−STEM images of gold−ceria catalysts: (a,b) 1% Au/CeO_2; (c,d) 0.5% Au/CeO_2. Yellow circles: typical Au single atoms.

The oxidation state of gold in both gold−ceria catalysts was also investigated by XPS analysis. As shown in Figure 2b, a doublet assigned to Au^+ between 88.1 and 84.2 eV was observed in the Au 4f spectra,[41−43] suggesting that the same electronic state of gold existed in both catalysts. Thus, based on the structure characterizations and analysis described above, here, two comparable gold single atom structures were fabricated on the nanoceria matrix.

3.2. Catalytic Activity Evaluation. For gold catalysts, a lot of works focused on fundamental issues have been studied, including the authentic active site[44−50] and reaction pathways.[51−53] Au NPs (>2 nm) and subnanometric Au clusters were found to be much superior to gold single atoms in catalyzing low-temperature (L-T) CO oxidation.[54−56] However, the insight into catalytic behavior of distinctive single atoms is still limited so far. Thus, here, we constructed a comparable system and evaluated the performance of both atomically dispersed gold catalysts with different gold loadings in catalyzing CO oxidation. During the transient light off test (Figure 3a), the initial reactivity of 1% Au/CeO_2 emerged at low temperatures (below 30 °C) and CO totally converted to CO_2 at about 40 °C (heating rate: 2 °C·min^{-1}). The 0.5% Au/CeO_2 catalyst, in contrast, was still inactive at temperatures up to 45 °C, and the complete CO conversion was achieved at 70 °C. For comparison, we also evaluated the activity of the 0.2% Au/CeO_2 catalyst (Figure S3). In this case, it was hardly active for the CO oxidation at temperatures below 80 °C under the present reaction conditions (1% CO/20% O_2/N_2). Overall, the results for the Au/CeO_2 are well in line with the findings in previous studies.[57] The change of the activity with time on

DOI: 10.1021/acs.jpcc.9b00096
J. Phys. Chem. C 2019, 123, 9001−9012

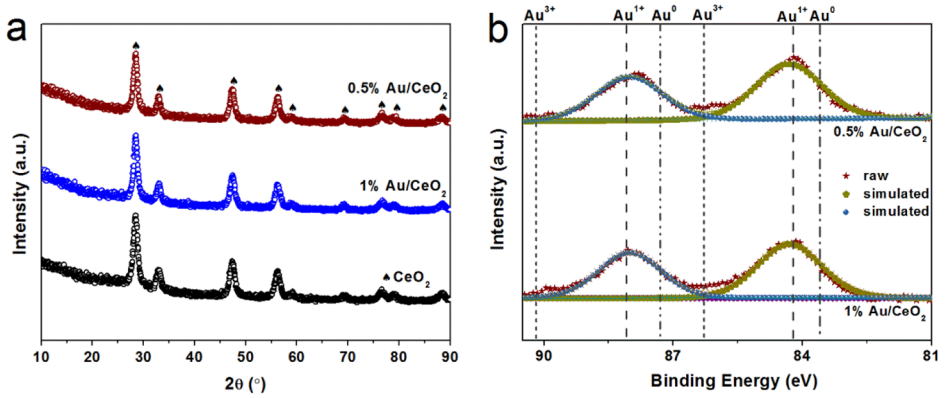

Figure 2. (a) XRD patterns and (b) XPS spectra of Au 4f of gold−ceria samples.

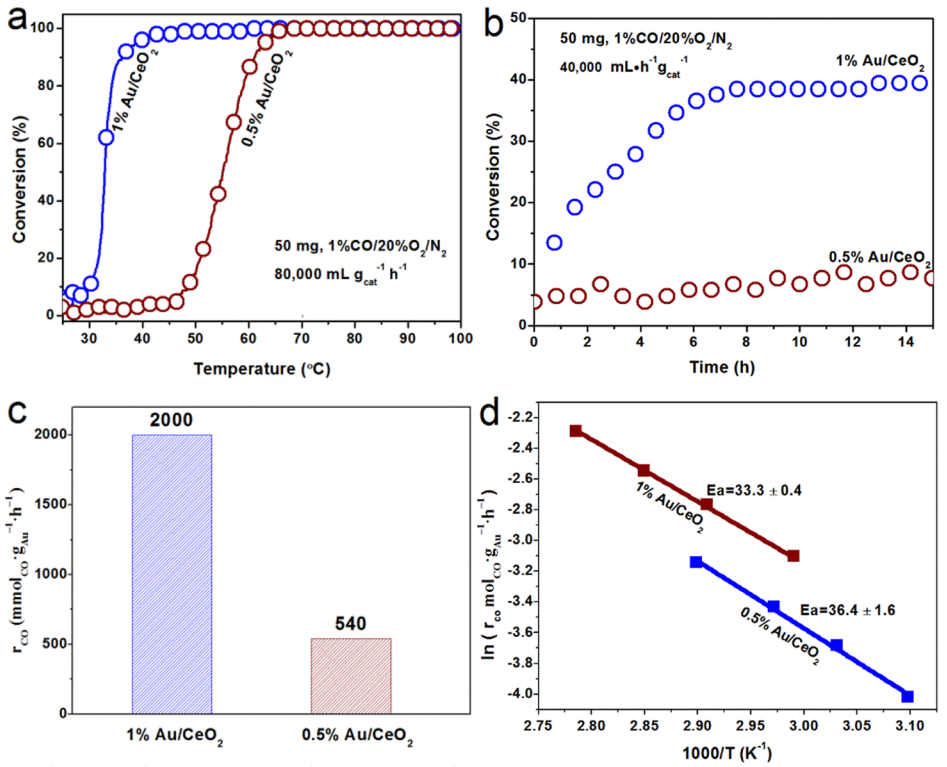

Figure 3. (a) CO conversions as a function of reaction temperature over gold−ceria catalysts. (b) Stability test lasting for 12 h at RT (25 °C). (c) CO reaction rate based on per gram Au. (d) Apparent activation energy (E_a).

stream at RT further allowed us to distinguish activity of both catalysts. As shown in Figure 3b, much distinct difference in catalytic performance was found over the two kinds of atomically dispersed gold catalysts. The activity of 0.5% Au/CeO_2 stabilized at a CO conversion value of 5% during the whole testing process. However, the 1% Au/CeO_2 catalyst exhibited an obvious gradual activation. The CO conversion increased all the time and ultimately reached a maximum value of 30−40% at about 8 h. In addition, as shown in Figure 3c, the reaction rate of 1% Au/CeO_2 normalized based on per gram Au amount was almost 4 times higher than that of 0.5% Au/CeO_2 (2000 vs 540 $mmol_{CO}{\cdot}g_{Au}^{-1}{\cdot}h^{-1}$) under the premise that CO conversion was controlled up to 12% at 40 °C by adjusting the SV. As shown in Figure 3d, the apparent activation energies (E_a) of the two catalysts were 33 and 36 $kJ{\cdot}mol^{-1}$ for 1% Au/CeO_2 and 0.5% Au/CeO_2, respectively, which were close to the values reported before.[57,58] The analogous E_a inferred that both catalysts might provide the same active site and obey the similar reaction pathway.[58−62] Overall, these results implied that significant differences in catalytic performance of both catalysts was not just induced by various gold loadings but was more attributed to intrinsic difference in gold species under the reaction condition.[60−62]

To explore the distinct difference in catalytic behaviors of these two kinds of atomically dispersed gold catalysts, the catalysts were further analyzed after CO oxidation stability lasted for 10 h at RT. As shown in Figure S4, very fine gold species were highly dispersed on the surface of the support for both spent catalysts and no gold particles were observed. HAADF−STEM images (Figure 4) showed that partial gold clusters can be observed on the surface of the spent 1% Au/CeO_2 catalyst. Conversely, no detectable changes emerged on the spent 0.5% Au/CeO_2 catalyst. From the XRD results, only diffraction peaks indexed to CeO_2 were examined, which is the

DOI: 10.1021/acs.jpcc.9b00096
J. Phys. Chem. C 2019, 123, 9001−9012

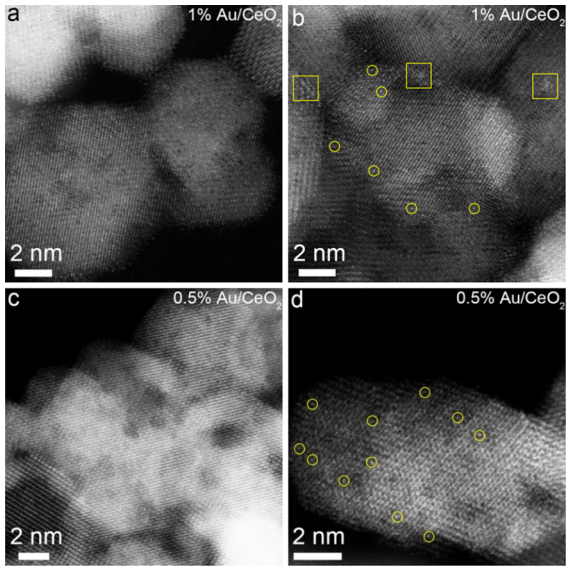

Figure 4. Aberration-corrected HAADF–STEM images of gold–ceria samples after the CO oxidation stability test: (a,b) 1% Au/CeO_2; (c,d) 0.5% Au/CeO_2. Yellow circles: Au single atoms. Yellow squares: Au clusters.

same to that of the fresh catalysts (Figure 5a). The XPS spectrum of the used 1% Au/CeO_2 sample showed that the oxidized gold species were transformed to the metallic state [Au(0)]. As expected, gold atoms in the 0.5% Au/CeO_2 sample remained as Au(I) (Figure 5b). For the 1% Au/CeO_2 sample, partial gold single atoms were aggregated into gold clusters, while few gold clusters existed in the used 0.5% Au/CeO_2 sample because of strong Au–O–Ce interaction. This interaction between gold species and ceria support for the 0.5% Au/CeO_2 catalyst was also proved by H_2-TPR results. As shown in Figure 6a, on the one hand, the reduction peak induced by the Au–Ce interaction for the 1% Au/CeO_2 sample centered at 130 °C, which was 20 °C lower than that of 0.5% Au/CeO_2. As for 0.2% Au/CeO_2, the reduction peak was centered at 174 °C (Figure S5), indicating the strongest interaction between the gold and ceria support among these three samples. This fact indicated that the distinct Au–Ce interactions caused different decentralized states of gold atoms in both the catalysts. On the other hand, the integral area of reduction peaks (hydrogen consumptions) for the both catalysts was quite similar (Table S1), indicating the more oxygen atoms activated efficiently by the gold atoms were anchored on the surface of CeO_2 because of the stronger gold–ceria interaction on 0.5% Au/CeO_2. The used catalysts exhibited a typical reductive peak corresponding to gold clusters (Figure 6b).

Based on the above off-line characterization results, we have concluded that the gold species transformed from atomically dispersed gold to gold clusters after the CO oxidation reaction for the 1% Au/CeO_2 catalyst, accompanying with a great enhancement in reactivity. In contrast, there was no distinct difference in the gold structure for the 0.5% Au/CeO_2 catalyst. More detailed evolution of the gold structure was in situ monitored by the DRIFTS. As shown in Figure 7, CO adsorption bands on the surface of the 1% Au/CeO_2 catalyst gradually shifted from 2154 to 2133 cm^{-1} with time on stream. Hadjiivanov et al. have demonstrated that the Au^{3+}–CO species are observed in the region of 2210–2170 cm^{-1} and assigned Au^{+}–CO to the range of 2190–2150 cm^{-1}.[63] The Au^{3+}–CO bond is virtually electrostatic; the corresponding gold carbonyls are easily decomposed. In contrast, Au^{+}–CO species exhibited higher stability resulting from the σ–π bond synergism.[63−65] Under the realistic reaction condition, Au^{+} species easily underwent reduction by the CO molecule.[66] Therefore, the adsorption peak at 2154 cm^{-1} was indexed to CO–Au^{n+} ($1 \leq n < 3$)[63−69] and 2133 cm^{-1} was assigned to CO–$Au^{\delta+}$ ($0 < \delta < 1$).[57,70,71] This result confirmed that during CO oxidation reaction, monodispersed gold atoms on the surface of the 1% Au/CeO_2 catalyst were unstable and transformed to clustered gold species. While for the 0.5% Au/CeO_2 catalyst, Au^{n+} was almost unchanged during the steady-state test condition. Meanwhile, this evidence perfectly explained the reason why distinct differences were performed in CO oxidation stability. Furthermore, it was worth noting that the generated CO_2 signal (2341 and 2361 cm^{-1}) was instantly increased for the 1% Au/CeO_2 catalyst with the gold structure transforming, while much weaker CO_2 response was detected for 0.5% Au/CeO_2 (Figure 7). To obtain a more convincing result, we further verified the gold species by in situ DRIFTS in the spent catalysts and at different temperatures under the reaction condition (Figures S6 and S7). The results of the steady state of 1% Au/CeO_2 indicated that clustered gold species were stable with increasing temperature. Similar gold structural transformation was exhibited at 50 °C for the 0.5% Au/CeO_2 catalyst, along with the increase in reactivity. At the same time, we conducted a second round test on catalytic activity and found that the second round of activity

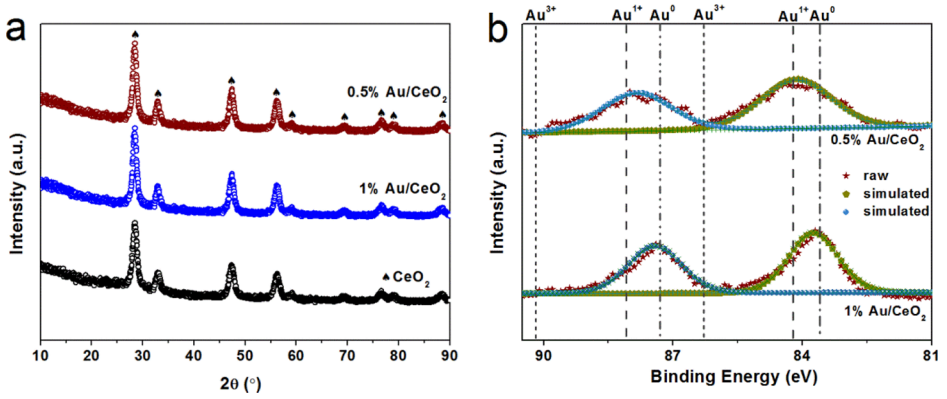

Figure 5. (a) XRD patterns and (b) XPS spectra of Au 4f of gold–ceria samples after the CO oxidation stability test.

DOI: 10.1021/acs.jpcc.9b00096
J. Phys. Chem. C 2019, 123, 9001–9012

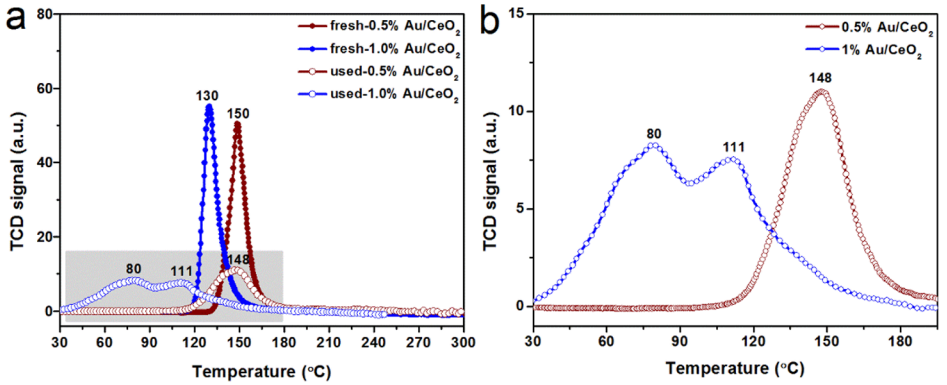

Figure 6. (a) H_2-TPR profiles over fresh and used for 10 h of Au/CeO_2 catalysts. (b) Magnified profiles of used Au/CeO_2 catalysts.

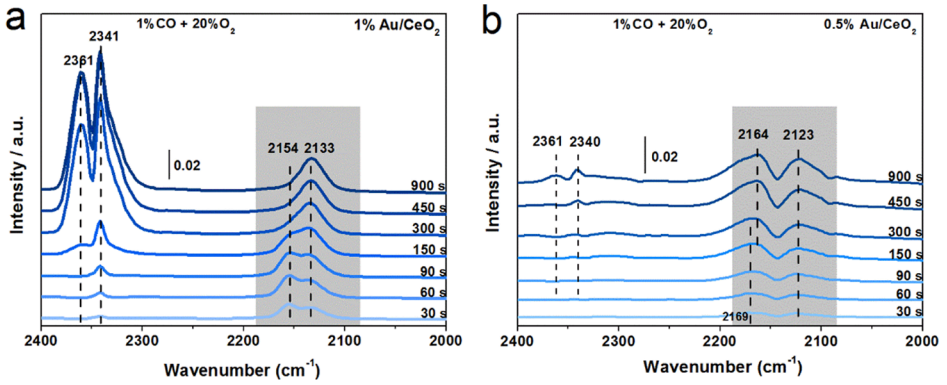

Figure 7. CO oxidation steady state study at 25 °C by in situ DRIFTS under mixed gas flow 1% CO/20% O_2/79% N_2 for (a) fresh 1% Au/CeO_2 and (b) fresh 0.5% Au/CeO_2, respectively. Reaction condition: the samples were in situ pretreated at 300 °C under air flow before data recorded (M = 30 mg, F = 30 mL·min^{-1}, T = 25 °C).

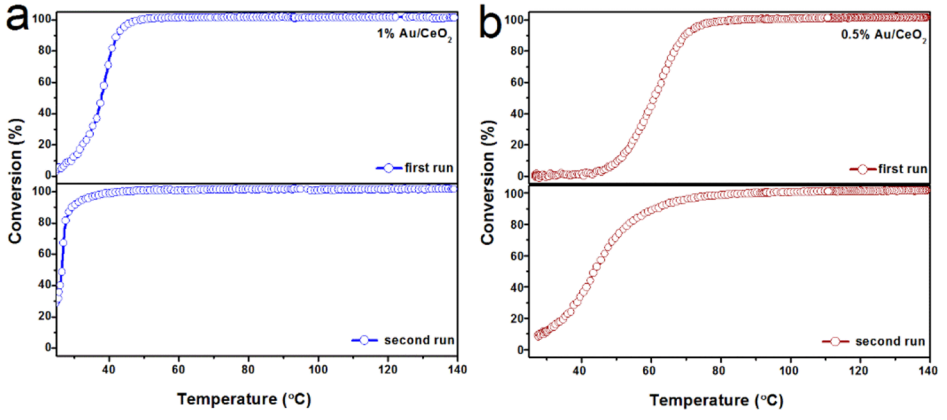

Figure 8. CO conversion over gold−ceria catalysts under light-off conditions for two runs: (a) 1% Au/CeO_2; (b) 0.5% Au/CeO_2 (80 000 mL·g_{cat}^{-1}·h^{-1}, 1% CO/20% O_2/79% N_2).

was much higher than that of the first round (Figure 8). In addition, a control experiment was conducted that strongly anchored gold atoms in 0.5% Au/CeO_2 were forced to aggregate into the gold cluster under the reducing atmosphere (2% CO/He), and the activity of CO oxidation was significantly enhanced (Figure S8). The above facts clearly evidenced that $Au^{\delta+}$ ($0 < \delta < 1$) performed a much more crucial role compared with Au^{n+} ($1 \leq n < 3$) in catalyzing CO oxidation.

To get more insight into the active surface species of both catalysts, we further performed the in situ CO adsorption experiment. The fresh catalysts were exposed to various feed gases following the sequence of CO−N_2−CO−O_2. For these highly dispersed Au atoms in the 1% Au/CeO_2 catalyst, in the first round adsorption at RT (Figure 9a), the CO finally adsorbed on clustered $Au^{\delta+}$ sites at 2127 cm^{-1} at 30 min. It is noticed that the intensity ratio of the band at 2127 cm^{-1} to that at 2169 cm^{-1} increased with increasing adsorption time, meaning that isolated Au atoms aggregated to form clusters gradually. Then, N_2 was used to flush the catalyst for another CO adsorption (Figure 9b), during which the CO−$Au^{\delta+}$ band at 2127 cm^{-1} disappeared because of the CO desorption. In the CO adsorption for the second time (Figure 9c), the intensity ratio of the band at 2127 cm^{-1} to that at 2169 cm^{-1}

DOI: 10.1021/acs.jpcc.9b00096
J. Phys. Chem. C 2019, 123, 9001−9012

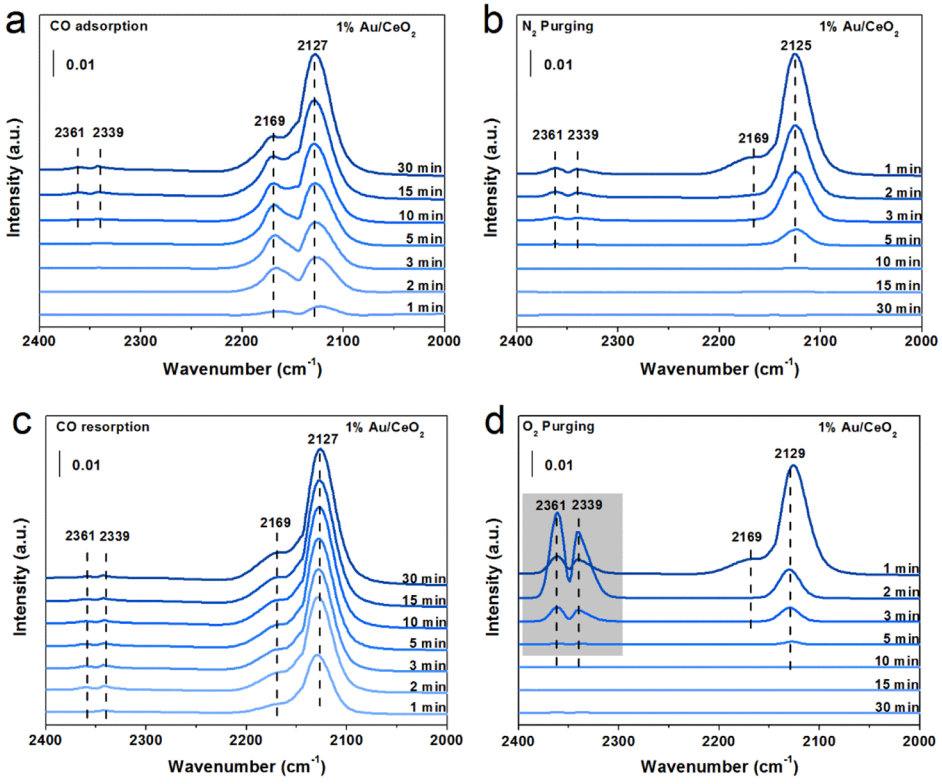

Figure 9. In situ DRIFTS study of 1% Au/CeO_2 during the CO adsorption−desorption: (a) CO adsorption; (b) N_2 purging; (c) CO resorption; (d) O_2 removal. The catalysts were in situ pretreated as same as the catalytic test.

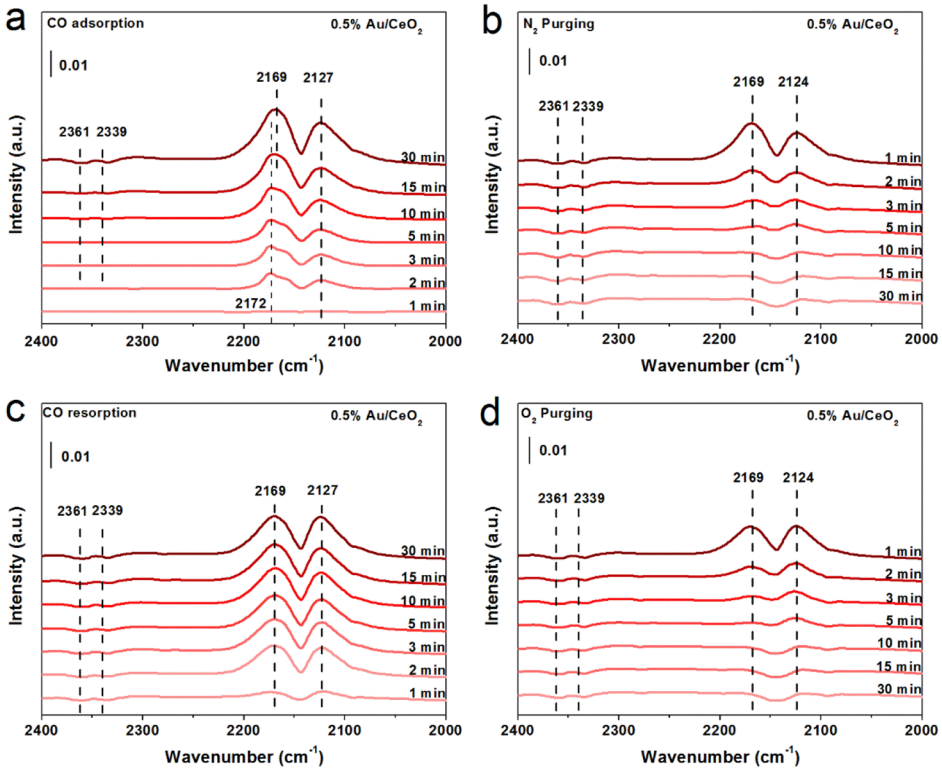

Figure 10. In situ DRIFTS study of 0.5% Au/CeO_2 during the CO adsorption−desorption: (a) CO adsorption; (b) N_2 purging; (c) CO resorption; and (d) O_2 removal. The catalysts were in situ pretreated as same as catalytic test.

was roughly constant, indicating the irreversible change of gold species from single atoms to clusters for the 1% Au/CeO_2 catalyst. Comparing the physical CO desorption during N_2 purging (Figure 9b), reaction of CO−$Au^{\delta+}$ at 2127 cm^{-1} with O_2 under O_2/N_2 purging was proven by the much faster disappearance of adsorbed CO, the abundant CO_2 generation

DOI: 10.1021/acs.jpcc.9b00096
J. Phys. Chem. C 2019, 123, 9001−9012

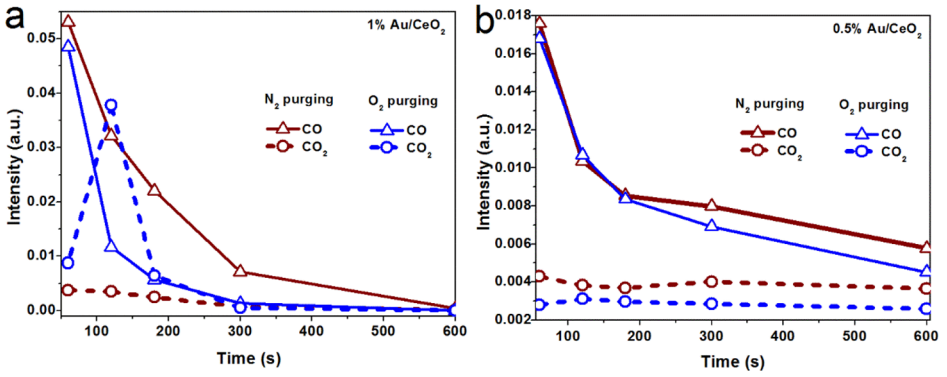

Figure 11. Relative peak intensities of CO and CO_2 in CO adsorption−desorption collected during the N_2 purging or O_2 removal stages after CO saturated adsorption: (a) 1% Au/CeO_2 and (b) 0.5% Au/CeO_2.

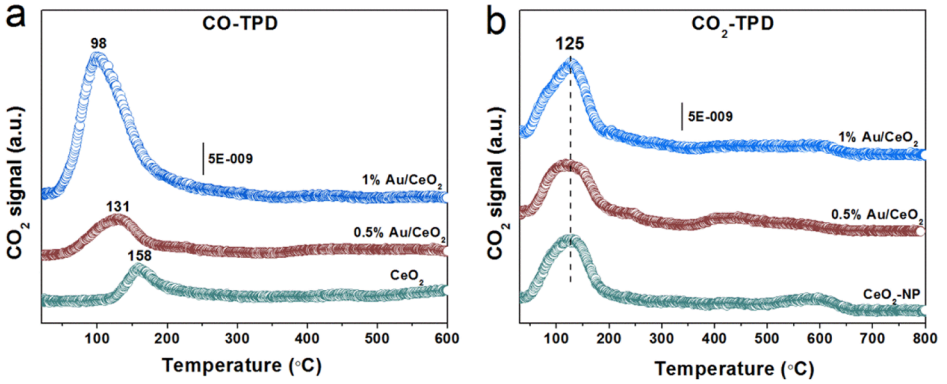

Figure 12. (a) CO-TPD profiles and (b) CO_2-TPD profiles of CeO_2, 0.5% Au/CeO_2, and 1% Au/CeO_2 catalysts.

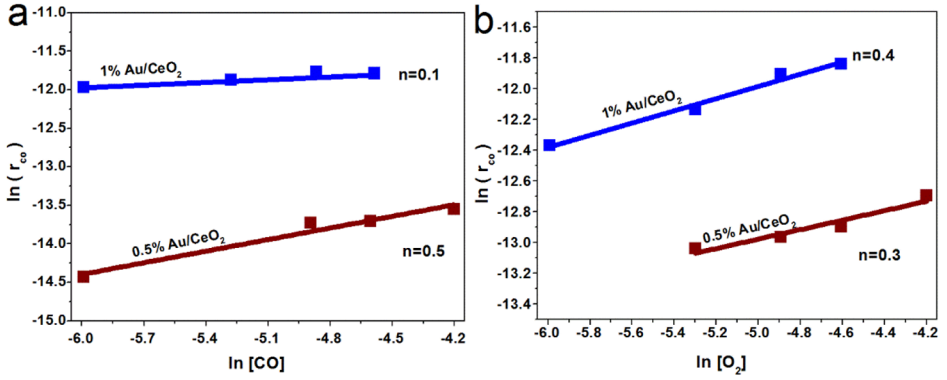

Figure 13. Kinetics reaction orders of (a) CO and (b) O_2 for 0.5% Au/CeO_2 and 1% Au/CeO_2 catalysts.

(Figure 9d). In contrast, one much weaker CO adsorption was observed for the 0.5% Au/CeO_2 catalyst (Figure 10a). CO desorption was observed in N_2 purging (Figure 10b). For the re-adsorption of CO after N_2 purging (Figure 10c), no obviously enhanced CO−$Au^{\delta+}$ at 2127 cm^{-1} was observed compared with that in CO adsorption for the first round. This means the highly dispersed gold atoms in 0.5% Au/CeO_2 were very stable during the CO adsorption at RT. Correspondingly, there was no CO_2 output for the 0.5% Au/CeO_2 catalyst after O_2 supplying (Figure 10d). The results on intensity statistics of adsorbed peaks showed this difference more vividly (Figure 11). A distinct response of CO_2 only occurred for clustered gold species in the 1% Au/CeO_2 catalyst, together with one steeper slope under the O_2 purging (blue solid line). The results of the CO adsorption test at different temperatures (Figure S9) indicated that gold species of both catalysts were reduced by CO with the increasing temperature. These above distinctions for the two catalysts convincingly proved the particular contribution of CO−$Au^{\delta+}$ in reacting with O_2, even at a lower temperature (Figure S10). The DRIFTS results from 0.2% Au/CeO_2 also reflected that atomically dispersed gold atoms performed inferior in catalyzing CO oxidation (Figure S11).

In addition, to observe the desorption behavior of CO and CO_2 adsorbates, the temperature-programmed desorption of CO and CO_2 (CO-TPD and CO_2-TPD) was also investigated (Figure 12). After saturating CO adsorption at RT, CO_2 signals were detected for all the tested samples (1% Au/CeO_2, 0.5% Au/CeO_2, and CeO_2 support), indicating that adsorbed CO was oxidized to CO_2 in the subsequent

DOI: 10.1021/acs.jpcc.9b00096
J. Phys. Chem. C 2019, 123, 9001−9012

desorption process by the reactive oxygen on the surface of these catalysts (Figure 12a). The integrated areas of the generated CO_2 signal from CO-TPD profiles for 1% Au/CeO_2 were much larger than that of 0.5% Au/CeO_2. This fact elucidated that 1% Au/CeO_2 was superior in the adsorbing CO reagent compared to 0.5% Au/CeO_2 (Figure S12), which was well in line with above in situ DRIFTS CO adsorption behaviors. On the other hand, after sufficiently adsorbing CO_2 feed gas, the desorption behavior of CO_2 (m/z = 44) for both gold−ceria samples resembled with pure CeO_2 support (Figure 12b), suggesting the comparable ability to CO_2 desorption for both catalysts. Therefore, we can conclude that the superiority in CO adsorption might be the key factor to the high reaction rate for 1% Au/CeO_2.

Similar results were also confirmed by the kinetic studies. As shown in Figure 13a, the 1% Au/CeO_2 catalyst showed very small n_{CO} values (n_{CO} = 0.1), illustrating the superiority in CO adsorption of the clustered structure of gold. However, the CO reaction order (n_{CO} = 0.5) for 0.5% Au/CeO_2 was much larger than that of 1% Au/CeO_2, implying insufficiency of effective CO adsorption during CO reaction. Taking into account that O_2 adsorption and activation is another key step for CO oxidation reaction, we further tried to identify the role of O_2. The O_2 reaction order was almost equivalent for 0.5% Au/CeO_2 (n_{O_2} = 0.3) and 1% Au/CeO_2 (n_{O_2} = 0.4), which inferred that the O_2 coverage played a minor role in inducing the catalytic performance gap here (Figure 13b). This is well in line with the results from Raman spectra and CO-TPR (Figures S13 and S14). It has been well proved that the O_2 activation step was strongly related to surface O-vacancies,[12,70−72] which corresponded to the induced defect mode (I_D) peak at ∼560 cm^{-1}. For both catalysts, there was no detectable difference in the Raman spectra between 0.5% Au/CeO_2 and 1% Au/CeO_2 collected before and after the catalytic reaction, indicating that the ability of both the catalysts to provide reactive oxygen was comparable.

4. DISCUSSION

4.1. Structural Characteristics of the Au/CeO_2 Catalyst. Two kinds of atomically dispersed Au/CeO_2 catalysts possessed similar specific surface areas (Figure S1). TEM images and XRD diffraction results showed that gold atoms uniformly dispersed on the surface of both catalysts. XPS analysis of both fresh catalysts was demonstrated in Figure 2b. The same electronic state of gold existed in both catalysts. Overall, the structure of the two catalysts is comparable.

The Au−O−Ce interaction has been investigated by the TPR (Figure 6). Both catalysts performed reduction peaks at different positions, and the 1% Au/CeO_2 sample was easier to be reduced than the 0.5% Au/CeO_2 sample, showing that gold atoms might be anchored at different sites on both the catalysts.[73] Meanwhile, this implied that the interactions of gold and CeO_2 were distinguishing in two catalysts. This deduction agreed with Corma's work.[8,74] Corma et al. reported that the interaction with the support might induce different particle shapes, and the metal oxide support could modify the properties of gold species deposited on it.[74] Moreover, the particle shape might be noticeably distorted with the continuous interaction of the low-coordinated gold atoms and support.[75] In addition, gold NPs became positively charged when supported on stoichiometric metal oxide surfaces and negatively charged when loaded on reduced surfaces.[73−77] On the stoichiometric support, the Au−O interaction was weak, while the Au−O interaction was strong enough on the reduced Au/TiO_2 catalyst, simulated by the Au_{13}/TiO_2-O_{vac} model.[75] The situation is analogous but not completely equivalent. According to the different interaction, we speculated that these weakly bound gold species in 1% Au/CeO_2 may be anchored at a stoichiometric CeO_2 surface, while strongly bound gold species in 0.5% Au/CeO_2 may be anchored at a reduced CeO_2 surface (CeO_2-O_{vac} model). This also coincided with the conjecture that charge transfer occurred between Au and CeO_2 support could modify the electronic structure of supported Au particles.[57] This requires us further investigations. Therefore, the distinguishing interactions induced different decentralized states of gold atoms in both the catalysts under the reaction condition. Meanwhile, the results of XPS analysis (Figures 2b and 5b) suggested gold particles presented in the used 1% Au/CeO_2 sample because of weak Au−O−Ce interaction, while only gold atoms existed in the used 0.5% Au/CeO_2 resulting from strong Au−O−Ce interaction.

4.2. Identification of Active Sites under the Reaction Condition. HAADF−STEM images over spent catalysts in Figure 4 exhibited the presence of gold clusters in 1% Au/CeO_2, indicating a part of gold single atoms were reduced to gold clusters, while gold single atoms were unchanged in 0.5% Au/CeO_2. The evolution of gold species is consistent with the above results of XPS analysis. More intuitive and detailed evolution of the gold structure under the reaction condition was monitored by in situ DRIFTS. Figure 7 exhibited that activity was instantly increased for the 1% Au/CeO_2 catalyst with the gold structure transforming from $CO-Au^{n+}$ ($1 \le n < 3$) to $CO-Au^{\delta+}$ ($0 < \delta < 1$). However, 0.5% Au/CeO_2 with $CO-Au^{n+}$ ($1 \le n < 3$) species was almost inactive for CO oxidation at 25 °C. Similar gold structural transformation was observed at 50 °C along with the increase in reactivity. The evidences clearly proved that $Au^{\delta+}$ performed much more crucial compared with Au^{n+} in catalyzing CO oxidation. Therefore, we have concluded that the high activity of 1% Au/CeO_2 originated from the structure transformation of gold species from Au^{n+} ($1 \le n < 3$) to $Au^{\delta+}$ ($0 < \delta < 1$). While 0.5% Au/CeO_2 was inactive at the RT because of the strong interaction between the gold atoms and ceria, which makes it difficult to be activated, as shown in Scheme 1.

4.3. Adsorption−Desorption Behavior of Atomically Dispersed Gold Species. For CO oxidation reaction,

Scheme 1. Schematic Diagram of the Gold Species Structural Evolution under CO Oxidation Condition at RT for 1% Au/CeO_2 and 0.5% Au/CeO_2 Catalysts

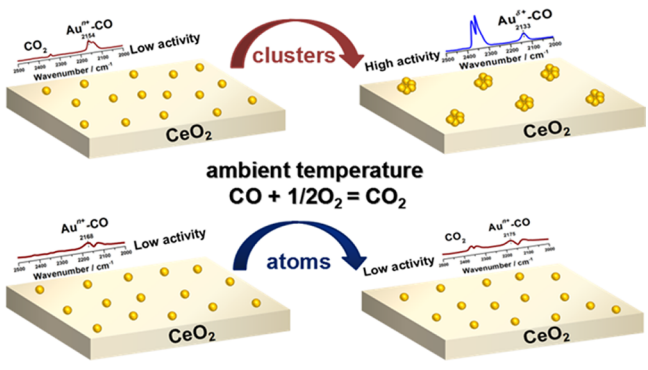

DOI: 10.1021/acs.jpcc.9b00096
J. Phys. Chem. C 2019, 123, 9001−9012

adsorption−desorption abilities of reactants CO and O_2 were very essential.[67] In terms of O_2 adsorption and activation, there was almost no significant difference in Raman spectra (Figure S11) for both the catalysts. The O_2 reaction orders were almost equivalent (0.3 vs 0.4). Therefore, O_2 activation may not be a key factor in causing differences in activity. The in situ DRIFTS study of CO adsorption−desorption over Au/CeO_2 in Figures 10 and 11 showed CO−$Au^{\delta+}$ in 2127 cm^{-1} performed superior ability to adsorb CO compared with CO−Au^{n+} at 25 °C. Even at a lower temperature (Figure S9), the gold cluster was active and displayed strong CO adsorption behavior, which was well in line with the phenomenon of CO-TPD. The kinetics studies further verified the superiority in CO adsorption of the clustered structure of gold because of small CO reaction order n_{CO} values (n_{CO} = 0.1) relative to (n_{CO} = 0.5) that of the 0.5% Au/CeO_2.

5. CONCLUSIONS

In summary, we executed a systematic investigation into the intrinsic contribution and structure evolution of atomically dispersed gold on ceria in catalyzing CO oxidation. Two kinds of gold atoms dispersed on the nanopolyhedron ceria exhibited distinct behaviors in catalyzing CO oxidation. A part of the isolated Au atoms in the 1% Au/CeO_2 catalyst were easier to agglomerate and transform to Au clusters under the reaction condition because of the weak interaction, which greatly enhanced the ability to capture CO molecules at $Au^{\delta+}$ ($0 < \delta < 1$) sites. In contrast, these strongly anchored Au single atoms in the 0.5% Au/CeO_2 catalyst were inferior in adsorbing CO molecules, which dominantly restricted their catalytic activity.

■ ASSOCIATED CONTENT

Supporting Information

The Supporting Information is available free of charge on the ACS Publications website at DOI: 10.1021/acs.jpcc.9b00096.

ICP-AES analysis; HRTEM images; STEM-EDS mapping; N_2 adsorption−desorption isotherms; control experiment; reference catalytic activity and H_2-TPR; additional in situ DRIFTS; ex situ Raman spectra; and CO-TPR profiles (PDF)

■ AUTHOR INFORMATION

Corresponding Authors

*E-mail: cma@hnu.edu.cn (C.M.).
*E-mail: sirui@sinap.ac.cn (R.S.).
*E-mail: jiacj@sdu.edu.cn (C.-J.J.).

ORCID

Chao Ma: 0000-0001-8599-9340
Chun-Jiang Jia: 0000-0002-4254-5100

Notes

The authors declare no competing financial interest.

■ ACKNOWLEDGMENTS

We acknowledge financial support from the Excellent Young Scientists Fund from the National Natural Science Foundation of China (NSFC) (grant no. 21622106), other projects from the NSFC (grant nos. 21773288, 21805167 and 21771117), the Outstanding Scholar Fund (grant no. JQ201703) and the Doctoral Fund (grant no. ZR2018BB010) from the Science Foundation of Shandong Province of China, the Taishan Scholar Project of Shandong Province of China, the Hundred Talents project of the Chinese Academy of Sciences and the Foundation of State Key Laboratory of Coal Conversion (grant nos. J17-18-902). We thank the Center of Structural Characterizations and Property Measurements at Shandong University for the help on sample characterizations.

■ REFERENCES

(1) Haruta, M.; Kobayashi, T.; Sano, H.; Yamada, N. Novel Gold Catalysts for the Oxidation of Carbon Monoxide at a Temperature far Below 0 °C. *Chem. Lett.* **1987**, *16*, 405−408.
(2) Chen, M. S.; Goodman, D. W. The Structure of Catalytically Active Gold on Titania. *Science* **2004**, *306*, 252−255.
(3) Rodriguez, J. A.; Ma, S.; Liu, P.; Hrbek, J.; Evans, J.; Perez, M. Activity of CeO_x and TiO_x Nanoparticles Grown on Au(111) in the Water-Gas Shift Reaction. *Science* **2007**, *318*, 1757−1760.
(4) Janssens, T. V. W.; Clausen, B. S.; Hvolbæk, B.; Falsig, H.; Christensen, C. H.; Bligaard, T.; Nørskov, J. K. Insights Into the Reactivity of Supported Au Nanoparticles: Combining Theory and Experiments. *Top. Catal.* **2007**, *44*, 15−26.
(5) Green, I. X.; Tang, W.; Neurock, M.; Yates, J. T. Spectroscopic Observation of Dual Catalytic Sites during Oxidation of CO on a Au/TiO_2 Catalyst. *Science* **2011**, *333*, 736−739.
(6) Herzing, A. A.; Kiely, C. J.; Carley, A. F.; Landon, P.; Hutchings, G. J. Identification of Active Gold Nanoclusters on Iron Oxide Supports for CO Oxidation. *Science* **2008**, *321*, 1331−1335.
(7) Guzman, J.; Gates, B. C. Catalysis by Supported Gold: Correlation between Catalytic Activity for CO Oxidation and Oxidation States of Gold. *J. Am. Chem. Soc.* **2004**, *126*, 2672−2673.
(8) Carrettin, S.; Concepción, P.; Corma, A.; López Nieto, J. M.; Puntes, V. F. Nanocrystalline CeO_2 Increases the Activity of Au for CO Oxidation by Two Orders of Magnitude. *Angew. Chem., Int. Ed.* **2004**, *43*, 2538−2540.
(9) Si, R.; Flytzani-Stephanopoulos, M. Shape and Crystal-Plane Effects of Nanoscale Ceria on the Activity of $Au-CeO_2$ Catalysts for the Water-Gas Shift Reaction. *Angew. Chem.* **2008**, *120*, 2926−2929.
(10) Tang, H.; Wei, J.; Liu, F.; Qiao, B.; Pan, X.; Li, L.; Liu, J.; Wang, J.; Zhang, T. Strong Metal-Support Interactions between Gold Nanoparticles and Nonoxides. *J. Am. Chem. Soc.* **2015**, *138*, 56−59.
(11) Bond, G. C.; Thompson, D. T. Gold-Catalysed Oxidation of Carbon Monoxide. *Gold Bull.* **2000**, *33*, 41−50.
(12) Haruta, M. Spiers Memorial Lecture : Role of perimeter interfaces in catalysis by gold nanoparticles. *Faraday Discuss.* **2011**, *152*, 11−32.
(13) Valden, M.; Lai, X.; Goodman, D. W. Onset of Catalytic Activity of Gold Clusters on Titania with the Appearance of Nonmetallic Properties. *Science* **1998**, *281*, 1647−1650.
(14) Chen, M.; Goodman, D. W. Catalytically Active Gold on Ordered Titania Supports. *Chem. Soc. Rev.* **2008**, *37*, 1860−1870.
(15) Liu, Y.; Jia, C.-J.; Yamasaki, J.; Terasaki, O.; Schüth, F. Highly Active Iron Oxide Supported Gold Catalysts for CO Oxidation: How Small must the Gold Nanoparticles be? *Angew. Chem., Int. Ed.* **2010**, *49*, 5771−5775.
(16) Fierro-Gonzalez, J. C.; Gates, B. C.; Gates, B. C. "Mononuclear Au^{III} and Au^{I} Complexes Bonded to Zeolite NaY: Catalysts for CO Oxidation at 298 K.". *J. Phys. Chem. B* **2004**, *108*, 16999−17002.
(17) Qiao, B.; Wang, A.; Yang, X.; Allard, L. F.; Jiang, Z.; Cui, Y.; Liu, J.; Li, J.; Zhang, T. Single-Atom Catalysis of CO Oxidation using Pt_1/FeO_x. *Nat. Chem.* **2011**, *3*, 634−641.
(18) Thomas, J. M.; Saghi, Z.; Gai, P. L. Can a Single Atom serve as the Active Site in some Heterogeneous Catalysts? *Top. Catal.* **2011**, *54*, 588−594.
(19) Ranocchiari, M.; Lothschutz, C.; Grolimund, D.; van Bokhoven, J. A. Single-Atom Active Sites on Metal-Organic Frameworks. *Proc. R. Soc. A* **2012**, *468*, 1985−1999.
(20) Flytzani-Stephanopoulos, M.; Gates, B. C. Atomically Dispersed Supported Metal Catalysts. *Annu. Rev. Chem. Biomol. Eng.* **2012**, *3*, 545−574.

DOI: 10.1021/acs.jpcc.9b00096
J. Phys. Chem. C 2019, 123, 9001−9012

(21) Yang, X.-F.; Wang, A.; Qiao, B.; Li, J.; Liu, J.; Zhang, T. Single-Atom Catalysts: A New Frontier in Heterogeneous Catalysis. *Acc. Chem. Res.* **2013**, *46*, 1740−1748.
(22) Remediakis, I. N.; Lopez, N.; Nørskov, J. K. CO Oxidation on Rutile-Supported Au Nanoparticles. *Angew. Chem., Int. Ed.* **2005**, *44*, 1824−1826.
(23) Ouyang, R.; Liu, J.-X.; Li, W.-X. Atomistic Theory of Ostwald Ripening and Disintegration of Supported Metal Particles under Reaction Conditions. *J. Am. Chem. Soc.* **2012**, *135*, 1760−1771.
(24) Song, W.; Hensen, E. J. M. Structure Sensitivity in CO Oxidation by a Single Au Atom Supported on Ceria. *J. Phys. Chem. C* **2013**, *117*, 7721−7726.
(25) Liu, J.-C.; Wang, Y.-G.; Li, J. Toward Rational Design of Oxide-Supported Single-Atom Catalysts: Atomic Dispersion of Gold on Ceria. *J. Am. Chem. Soc.* **2017**, *139*, 6190−6199.
(26) Qiao, B.; Liang, J.-X.; Wang, A.; Xu, C.-Q.; Li, J.; Zhang, T.; Liu, J. J. Ultrastable single-atom gold catalysts with strong covalent metal-support interaction (CMSI). *Nano Res.* **2015**, *8*, 2913−2924.
(27) Qiao, B.; Liu, J.; Wang, Y.-G.; Lin, Q.; Liu, X.; Wang, A.; Li, J.; Zhang, T.; Liu, J. Highly Efficient Catalysis of Preferential Oxidation of CO in H_2-rich Stream by Gold Single-Atom Catalysts. *ACS Catal.* **2015**, *5*, 6249−6254.
(28) Wang, Y.-G.; Yoon, Y.; Glezakou, V.-A.; Li, J.; Rousseau, R. The Role of Reducible Oxide−Metal Cluster Charge Transfer in Catalytic Processes: New Insights on the Catalytic Mechanism of CO Oxidation on Au/TiO_2 from ab Initio Molecular Dynamics. *J. Am. Chem. Soc.* **2013**, *135*, 10673−10683.
(29) Wang, Y.-G.; Mei, D.; Glezakou, V.-A.; Li, J.; Rousseau, R. Dynamic Formation of Single-Atom Catalytic Active Sites on Ceria-Supported Gold Nanoparticles. *Nat. Commun.* **2015**, *6*, 6511−6518.
(30) Aguilar-Guerrero, V.; Gates, B. C. Kinetics of CO Oxidation Catalyzed by Highly Dispersed CeO_2-Supported Gold. *J. Catal.* **2008**, *260*, 351−357.
(31) Deng, W.; Carpenter, C.; Yi, N.; Flytzani-Stephanopoulos, M. Comparison of The Activity of Au/CeO_2 and Au/Fe_2O_3 Catalysts for the CO Oxidation and the Water-Gas Shift Reactions. *Top. Catal.* **2007**, *44*, 199−208.
(32) Wu, Z.; Zhou, S.; Zhu, H.; Dai, S.; Overbury, S. H. DRIFTS-QMS Study of Room Temperature CO Oxidation on Au/SiO_2 Catalyst: Nature and Role of Different Au Species. *J. Phys. Chem. C* **2009**, *113*, 3726−3734.
(33) Corma, A.; Concepción, P.; Boronat, M.; Sabater, M. J.; Navas, J.; Yacaman, M. J.; Larios, E.; Posadas, A.; López-Quintela, M. A.; Buceta, D.; et al. Exceptional Oxidation Activity with Size-Controlled Supported Gold Clusters of Low Atomicity. *Nat. Chem.* **2013**, *5*, 775−781.
(34) Landman, U.; Yoon, B.; Zhang, C.; Heiz, U.; Arenz, M. Factors in gold nanocatalysis: oxidation of CO in the non-scalable size regime. *Top. Catal.* **2007**, *44*, 145−158.
(35) Lu, J.; Aydin, C.; Browning, N. D.; Gates, B. C. Hydrogen Activation and Metal Hydride Formation Trigger Cluster Formation from Supported Iridium Complexes. *J. Am. Chem. Soc.* **2012**, *134*, 5022−5025.
(36) Liu, L.; Corma, A. Metal Catalysts for Heterogeneous Catalysis: from Single Atoms to Nanoclusters and Nanoparticles. *Chem. Rev.* **2018**, *118*, 4981−5079.
(37) Qi, L.; Yu, Q.; Dai, Y.; Tang, C.; Liu, L.; Zhang, H.; Gao, F.; Dong, L.; Chen, Y. Influence of Cerium Precursors on the Structure and Reducibility of Mesoporous $CuO-CeO_2$ Catalysts for CO Oxidation. *Appl. Catal., B* **2012**, *119-120*, 308−320.
(38) Haruta, M. Size- and Support-Dependency in the Catalysis of Gold. *Catal. Today* **1997**, *36*, 153−166.
(39) Yan, W.; Chen, B.; Mahurin, S. M.; Schwartz, V.; Mullins, D. R.; Lupini, A. R.; Pennycook, S. J.; Dai, S.; Overbury, S. H. Preparation and Comparison of Supported Gold Nanocatalysts on Anatase, Brookite, Rutile, and P25 Polymorphs of TiO_2 for Catalytic Oxidation of CO. *J. Phys. Chem. B* **2005**, *109*, 10676−10685.
(40) Liotta, L. F.; Di Carlo, G.; Pantaleo, G.; Venezia, A. M. Supported Gold Catalysts for CO Oxidation and Preferential Oxidation of CO in H_2 Stream: Support Effect. *Catal. Today* **2010**, *158*, 56−62.
(41) Sudarsanam, P.; Mallesham, B.; Reddy, P. S.; Grossmann, D.; Grünert, W.; Reddy, B. M. Nano-Au/CeO_2 Catalysts for CO Oxidation: Influence of Dopants (Fe, La and Zr) on the Physicochemical Properties and Catalytic Activity. *Appl. Catal., B* **2014**, *144*, 900−908.
(42) Zhang, X.; Shi, H.; Xu, B.-Q. Vital Roles of Hydroxyl Groups and Gold Oxidation States in Au/ZrO_2 Catalysts for 1, 3-Butadiene Hydrogenation. *J. Catal.* **2011**, *279*, 75−87.
(43) Ousmane, M.; Liotta, L. F.; Carlo, G. D.; Pantaleo, G.; Venezia, A. M.; Deganello, G.; Retailleau, L.; Boreave, A.; Giroir-Fendler, A. Supported Au Catalysts for Low-Temperature Abatement of Propene and Toluene, as model VOCs: Support Effect. *Appl. Catal., B* **2011**, *101*, 629−637.
(44) Li, M.; Wu, Z.; Ma, Z.; Schwartz, V.; Mullins, D. R.; Dai, S.; Overbury, S. H. CO Oxidation on $Au/FePO_4$ Catalyst: Reaction Pathways and Nature of Au Sites. *J. Catal.* **2009**, *266*, 98−105.
(45) Klimev, H.; Fajerwerg, K.; Chakarova, K.; Delannoy, L.; Louis, C.; Hadjiivanov, K. Oxidation of Gold Metal Particles Supported on TiO_2: an FTIR Study by Means of Low-Temperature CO Adsorption. *J. Mater. Sci.* **2007**, *42*, 3299−3306.
(46) Tibiletti, D.; Fonseca, A. A.; Burch, R.; Chen, Y.; Fisher, J. M.; Goguet, A.; Hardacre, C.; Hu, P.; Thompsett, D. DFT and In Situ EXAFS Investigation of Gold/Ceria−Zirconia Low-Temperature Water Gas Shift Catalysts: Identification of the Nature of the Active Form of Gold. *J. Phys. Chem. B* **2005**, *109*, 22553−22559.
(47) Haruta, M.; Tsubota, S.; Kobayashi, T.; Kageyama, H.; Genet, M. J.; Delmon, B. Low-Temperature Oxidation of CO over Gold Supported on TiO_2, α-Fe_2O_3, and Co_3O_4. *J. Catal.* **1993**, *144*, 175−192.
(48) Duan, Z.; Henkelman, G. Calculations of CO Oxidation over a Au/TiO_2 Catalyst: A Study of Active Sites, Catalyst Deactivation, and Moisture Effects. *ACS Catal.* **2018**, *8*, 1376−1383.
(49) Zhang, C.; Michaelides, A.; King, D. A.; Jenkins, S. J. Positive Charge States and Possible Polymorphism of Gold Nanoclusters on Reduced Ceria. *J. Am. Chem. Soc.* **2010**, *132*, 2175−2182.
(50) Aguilar-Guerrero, V.; Lobo-Lapidus, R. J.; Gates, B. C. Genesis of a Cerium Oxide Supported Gold Catalyst for CO Oxidation: Transformation of Mononuclear Gold Complexes into Clusters as Characterized by X-ray Absorption Spectroscopy. *J. Phys. Chem. C* **2009**, *113*, 3259−3269.
(51) Widmann, D.; Behm, R. J. Active Oxygen on a Au/TiO_2 Catalyst-Formation, Stability and CO Oxidation Activity. *Angew. Chem., Int. Ed.* **2011**, *50*, 10241−10245.
(52) Schlexer, P.; Widmann, D.; Behm, R. J.; Pacchioni, G. CO Oxidation on a Au/TiO_2 Nanoparticle Catalyst via the Au-assisted Mars-van Krevelen Mechanism. *ACS Catal.* **2018**, *8*, 6513−6525.
(53) Kim, H. Y.; Lee, H. M.; Henkelman, G. CO Oxidation Mechanism on CeO_2-Supported Au Nanoparticles. *J. Am. Chem. Soc.* **2012**, *134*, 1560−1570.
(54) Fu, Q.; Saltsburg, H.; Flytzani-Stephanopoulos, M. Active Nonmetallic Au and Pt Species on Ceria-Based Water-Gas Shift Catalysts. *Science* **2003**, *301*, 935−938.
(55) Jia, C.-J.; Liu, Y.; Bongard, H.; Schüth, F. Very Low Temperature CO Oxidation over Colloidally Deposited Gold Nanoparticles on $Mg(OH)_2$ and MgO. *J. Am. Chem. Soc.* **2010**, *132*, 1520−1522.
(56) Wang, J.; Tan, H.; Yu, S.; Zhou, K. Morphological Effects of Gold Clusters on the Reactivity of Ceria Surface Oxygen. *ACS Catal.* **2015**, *5*, 2873−2881.
(57) Chen, S.; Luo, L.; Jiang, Z.; Huang, W. Size-Dependent Reaction Pathways of Low Temperature CO Oxidation on Au/CeO_2 Catalysts. *ACS Catal.* **2015**, *5*, 1653−1662.
(58) Huang, X.-S.; Sun, H.; Wang, L.-C.; Liu, Y.-M.; Fan, K.-N.; Cao, Y. Morphology Effects of Nanoscale Ceria on the Activity of Au/CeO_2 Catalysts for Low-Temperature CO Oxidation. *Appl. Catal., B* **2009**, *90*, 224−232.

DOI: 10.1021/acs.jpcc.9b00096
J. Phys. Chem. C 2019, 123, 9001−9012

(59) El-Moemen, A. A.; Abdel-Mageed, A. M.; Bansmann, J.; Parlinska-Wojtan, M.; Behm, R. J.; Kučerová, G. Deactivation of Au/CeO_2 Catalysts during CO Oxidation: Influence of Pretreatment and Reaction Conditions. *J. Catal.* **2016**, *341*, 160−179.
(60) Xie, X.; Li, Y.; Liu, Z.-Q.; Haruta, M.; Shen, W. Low-Temperature Oxidation of CO Catalysed by Co_3O_4 nanorods. *Nature* **2009**, *458*, 746−749.
(61) Wang, F.; Li, C.; Zhang, X.; Wei, M.; Evans, D. G.; Duan, X. Catalytic Behavior of Supported Ru Nanoparticles on the {1 0 0},{1 1 0}, and {1 1 1} Facet of CeO_2. *J. Catal.* **2015**, *329*, 177−186.
(62) Cargnello, M.; Doan-Nguyen, V. V. T.; Gordon, T. R.; Diaz, R. E.; Stach, E. A.; Gorte, R. J.; Fornasiero, P.; Murray, C. B. Control of Metal Nanocrystal Size reveals Metal-Support Interface Role for Ceria Catalysts. *Science* **2013**, *341*, 771−773.
(63) Mihaylov, M.; Ivanova, E.; Hao, Y.; Hadjiivanov, K.; Knözinger, H.; Gates, B. C. ″Gold Supported on La_2O_3: Structure and Reactivity with CO_2 and Implications for CO Oxidation Catalysis. *J. Phys. Chem. C* **2008**, *112*, 18973−18983.
(64) Venkov, T.; Fajerwerg, K.; Delannoy, L.; Klimev, H.; Hadjiivanov, K.; Louis, C. Effect of the Activation Temperature on the State of Gold Supported on Titania: An FT-IR Spectroscopic Study. *Appl. Catal., A* **2006**, *301*, 106−114.
(65) Mihaylov, M.; Knözinger, H.; Hadjiivanov, K.; Gates, B. C. Characterization of the Oxidation States of Supported Gold Species by IR Spectroscopy of Adsorbed CO. *Chem. Ing. Tech.* **2007**, *79*, 795−806.
(66) Uzun, A.; Ortalan, V.; Browning, N. D.; Gates, B. C. A Site-Isolated Mononuclear Iridium Complex Catalyst Supported on MgO: Characterization by Spectroscopy and Aberration-Corrected Scanning Transmission Electron Microscopy. *J. Catal.* **2010**, *269*, 318−328.
(67) Green, I. X.; Tang, W.; McEntee, M.; Neurock, M.; Yates, J. T. Inhibition at Perimeter Sites of Au/TiO_2 Oxidation Catalyst by Reactant Oxygen. *J. Am. Chem. Soc.* **2012**, *134*, 12717−12723.
(68) Karpenko, A.; Leppelt, R.; Plzak, V.; Behm, R. The Role of Cationic Au^{3+} and Nonionic Au^0 Species in the Low-Temperature Water-Gas Shift Reaction on Au/CeO_2 Catalysts. *J. Catal.* **2007**, *252*, 231−242.
(69) Boccuzzi, F.; Chiorino, A.; Tsubota, S.; Haruta, M. FTIR Study of Carbon Monoxide Oxidation and Scrambling at Room Temperature over Gold supported on ZnO and TiO_2. *J. Phys. Chem.* **1996**, *100*, 3625−3631.
(70) Guzman, J.; Carrettin, S.; Corma, A. Spectroscopy Evidence for the Supply of Reactive Oxygen during CO Oxidation Catalyzed by Gold supported on Nanocrystalline CeO_2. *J. Am. Chem. Soc.* **2005**, *127*, 3286−3287.
(71) Widmann, D.; Behm, R. J. Activation of Molecular Oxygen and the Nature of the Active Oxygen Species for CO Oxidation on Oxide Supported Au Catalysts. *Acc. Chem. Res.* **2014**, *47*, 740−749.
(72) Yang, C.; Yu, X.; Heißler, S.; Weidler, P. G.; Nefedov, A.; Wang, Y.; Wöll, C.; Kropp, T.; Paier, J.; Sauer, J. O_2 Activation on Ceria Catalysts—The Importance of Substrate Crystallographic Orientation. *Angew. Chem., Int. Ed.* **2017**, *56*, 16399−16404.
(73) Boronat, M.; Illas, F.; Corma, A. Active Sites for H_2 Adsorption and Activation in Au/TiO_2 and the Role of the Support. *J. Phys. Chem. A* **2009**, *113*, 3750−3757.
(74) Guzman, J.; Carrettin, S.; Fierro-Gonzalez, J. C.; Hao, Y.; Gates, B. C.; Corma, A. CO Oxidation Catalyzed by Supported Gold: Cooperation between Gold and Nanocrystalline Rare-Earth Supports Forms Reactive Surface Superoxide and Peroxide Species. *Angew. Chem.* **2005**, *117*, 4856−4859.
(75) Boronat, M.; Corma, A. Oxygen Activation on Gold Nanoparticles: Separating the Influence of Particle Size, Particle Shape and Support Interaction. *Dalton Trans.* **2010**, *39*, 8538−8546.
(76) Carrettin, S.; Corma, A.; Iglesias, M.; Sánchez, F. Stabilization of Au(III) on Heterogeneous Catalysts and Their Catalytic Similarities with Homogeneous Au(III) Metal Organic Complexes. *Appl. Catal., A* **2005**, *291*, 247−252.
(77) Abad, A.; Concepción, P.; Corma, A.; García, H. A Collaborative Effect between Gold and a Support Induces the Selective Oxidation of Alcohols. *Angew. Chem., Int. Ed.* **2005**, *44*, 4066−4069.

DOI: 10.1021/acs.jpcc.9b00096
J. Phys. Chem. C 2019, 123, 9001−9012